Novel electrochemical sensor based on Fe$_3$O$_4$-ZrO$_2$-graphene oxide for determination of dopamine

Zhiyang Zhong[1] · Jiaojie Wang[1] · Shixin Jiang[1] · Menglu Li[1] · Jiaqi Lin[1] · Jie Pan[1] · Xiang Tao[1] · Aijuan Xie[1] · Shiping Luo[1]

Abstract

Graphene oxide (GO) was first prepared by an improved Hummers method; Fe$_3$O$_4$, ZrO$_2$, and corresponding metal oxide-GO composite materials were synthesized by a hydrothermal method. The electrochemical performance of as-prepared materials modified glassy carbon electrode (GCE) was investigated by cyclic voltammetry (CV). The ternary Fe$_3$O$_4$-ZrO$_2$-GO composite modified GCE was used as the electrochemical sensor for the dopamine (DA) detection. The CV test showed that the Fe$_3$O$_4$-ZrO$_2$-GO composite modified GCE had a good response to DA with good stability and reproducibility. Electrochemical impedance spectroscopy (EIS) illustrated that Fe$_3$O$_4$-ZrO$_2$-GO/GCE exhibited the lower R_{ct} value (14.11 Ω). Differential pulse voltammetry (DPV) test demonstrated that the ternary composite has excellent anti-interference ability. The linear relationship by differential pulse voltammetry for Fe$_3$O$_4$-ZrO$_2$-GO/GCE was $I_{pa}(\mu A) = 0.2552x + 0.0056$ ($R^2 = 0.9804$) with the sensitivity of 3.649 μA μM^{-1} cm^{-2} and detection limit of 0.1562 μM in the ranges of $0.5 - 15$ μM. The developed electrochemical sensor was successfully applied to the DA detection in human serum with satisfactory recovery rate. The possible synergistic amplification effect brought from Fe$_3$O$_4$, ZrO$_2$, and GO for DA detection was proposed based on experimental results.

Keywords Metal oxide · Graphene oxide · Hydrothermal method · Dopamine · Electrochemical sensor

Introduction

Dopamine (DA), found in the kidney, hormone system, and central nervous system, is a kind of catecholamine neurotransmitter [1]. It plays a key role for mankind in controlling behavior, emotion, cognition, and memory [2]. Abnormal concentration of DA in body fluid may lead to neurological diseases [3]. Therefore, it is very necessary to accurately, sensitively, and selectively detect DA in biological fluid. Currently, liquid chromatographic analysis (LC) [3], chemiluminescence analysis (CL), [4] fluorescence analysis (FL) [5, 6], capillary electrophoresis analysis (CE) [7], and UV–Vis spectroscopy [8] and other methods have been used for DA detection. Nevertheless, owing to the disadvantages of the large size of the device, high cost, lengthy pretreatment process, and complex operating conditions, the wide application of the above methods is limited. In contrast, electrochemical method has received extensive attention due to the outstanding advantages such as rapid determination, convenient operation, high sensitivity, and good selectivity [9]. The development of electrode materials with high electrochemical activity is a key issue in the construction of sensitive and accurate electrochemical sensors for DA detection [10].

Metal oxide usually has good sensitivity, cost-effectiveness, non-toxicity, and rapid response, and its chemical composition is relatively stable. Metal oxides are known for their ease of fabrication; they can be tailored into multiple nanostructures like nanorod [11], nanotube [12], nanowire [13], nanosphere [14], and nanoparticle [15]. If they are used as an electrode material, they can not only increase working time but also broaden the application environment of electrochemical sensors. Moreover, the various chemical valence states of metal oxides can provide space for redox reactions. Fe$_3$O$_4$ is a typical magnetic nanoparticle that has attracted widespread attention due to low cost, easy synthesis, superior electrocatalytic

✉ Aijuan Xie
aijuan_xie@126.com

✉ Shiping Luo
shiping_luo@163.com

1 School of Petrochemical Engineering, Changzhou University, Changzhou 213164, People's Republic of China

activity, and the advantages of environmental friendliness [16, 17], which allow them to be used in a variety of fields such as targeted drug delivery [18], biological imaging [19], and, in particular, electrochemical sensors [20]. However, it is difficult to prepare a uniform Fe_3O_4-modified electrochemical sensor due to the fact that they are prone to aggregation brought from the magnetic attraction between the dipoles. At the same time, the limited specific binding functional groups result in the reduction of electrocatalytic activity and the obstruction of electron transfer [21]. In addition, Fe_3O_4 is very likely to aggregate [22]. Studies have shown that the hybridization of Fe_3O_4 with other nanomaterials can prevent their aggregation, improve their chemical stability, and reduce their toxicity [23, 24]. Among which, carbon, conductive polymers, and metal oxides NPs can play a crucial role, thus enhancing the performance of electrochemical sensors [25]. Zirconium oxide, with a wide band gap of 5.0 eV, is chemically inactive with a high melting point, high resistivity, and low thermal expansion coefficient and has been widely used in piezoelectric materials [26], ceramic material [27], magnetic materials [28], and catalysts [29]. Due to the extreme chemical stability, ZrO_2 have been rarely reported as eletrochemical sensors for DA detection. The existing reports for sensors are mainly for gas sensors [30, 31]. In addition, ZrO_2 was used as excellent surface modifier to effectively improve the response to DA of ZrO_2-based electrochemical sensor. Graphene oxide (GO) are very promising materials for biosensors due to their low-cost fabrication, high surface area, and direct interaction with a variety of biomolecules. GO has both sp^2 and sp^3 hybridized carbon atoms, as well as different functional groups such as hydroxyl, carboxyl, and epoxy[32–35]. Furthermore, compared with graphene, GO can be dispersed in water, which is suitable for mass production [32], and the chemical structure of GO can be modified by chemical, thermal, or solvent thermal reduction methods [36], which is also valuable for biosensors due to its adjustable electronic and optical properties. [37]

Therefore, in this work, single-metal oxides (Fe_3O_4, ZrO_2) and GO are firstly prepared respectively, and then binary, ternary composites are synthesized in turn. Among which, GO is used as the substrate and loaded with two metal oxides. By taking advantage of the excellent conductivity of GO, the enhanced redox capacity of metal oxides, and the synergistic effect of the two metal oxides and GO, the composite can achieve the goal of high sensitivity, high selectivity, and excellent stability in the dopamine detection.

Experimental section

Reagents and apparatus

All chemicals were of analytical reagent grade and used directly without further treatment. Graphite powder was provided by Shenzhen Hanhui graphite Co. LTD (China). Ferrous sulfate heptahydrate ($FeSO_4 \cdot 7H_2O$), sodium hydroxide (NaOH), zirconium nitrate pentahydrate ($Zr(NO_3)_4 \cdot 5H_2O$), anhydrous sodium acetate (CH_3COONa), N,N-dimethylformamide (DMF), ethanol, and hydrochloric acid (HCl) were purchased from Sinopharm Chemical Reagent Co., LTD (Shanghai, China). All aqueous solutions were freshly prepared with deionized water.

X-ray diffraction (XRD) was obtained using D/Max 2500 PC X-ray diffractometer with Cu Kα radiation (Rigaku Corporation, Japan), while Fourier transform infrared spectroscopy (FTIR) spectrum was recorded using FTIR-8400S Fourier infrared spectrometer (Shimadzu, Japan). Scanning electron microscopy (SEM) images and energy dispersive X-ray analysis (EDS) data were obtained using Regulus-8100 (HITACHI, Japan). The X-ray photoelectron spectroscopy (XPS) was performed using an Omicron energy analyzer (AXIS, Shimadzu, Japan).

Synthesis of samples

Synthesis of GO

GO is prepared according to the improved Hummers method [38]. H_2SO_4 (~ 98%, 23 mL) was added to the mixture of graphite powder (1.0 g) and $NaNO_3$ (0.5 g), and the temperature of above mixture was cooled to 0 °C, then $KMnO_4$ (3.0 g) was slowly added in batches to keep the reaction temperature below 20 °C. Next, the reaction temperature was increased to 35 °C and stirred for 5 h, the additional $KMnO_4$ (3.0 g) was added in batches again. Then 140 mL of deionized water was added into it and stirred for 30 min, followed by adding 30% H_2O_2 (1.0 mL) until the mixture turned bright yellow, the mixture was centrifuged and the remaining solid substance was continuously washed with 30% HCl and water respectively until the pH was 4 − 5, and the resulting solids are dried in vacuum.

Synthesis of Fe_3O_4-GO

Ten milligram GO was added into 20 mL deionized water, which was dispersed by ultrasound for 30 min, then 10 mL $FeSO_4 \cdot 7H_2O$ solution (0.50 mol L^{-1}) was added to the above suspension under strenuous agitation. After adjusting pH to 10 with 0.50 mol L^{-1} NaOH solution, the suspension was transferred to a stainless steel autoclave and heated at 180 ℃ for 8 h. The resulting product was washed with ethanol and water, and then dried in a vacuum drying oven of 60 ℃ to constant weight. The synthesis method of Fe_3O_4 was the same as the above steps, except that GO was not added in the first step.

Scheme 1 Schematic representation of the fabrication process for Fe₃O₄- ZrO₂-GO/GCE and main test methods to DA
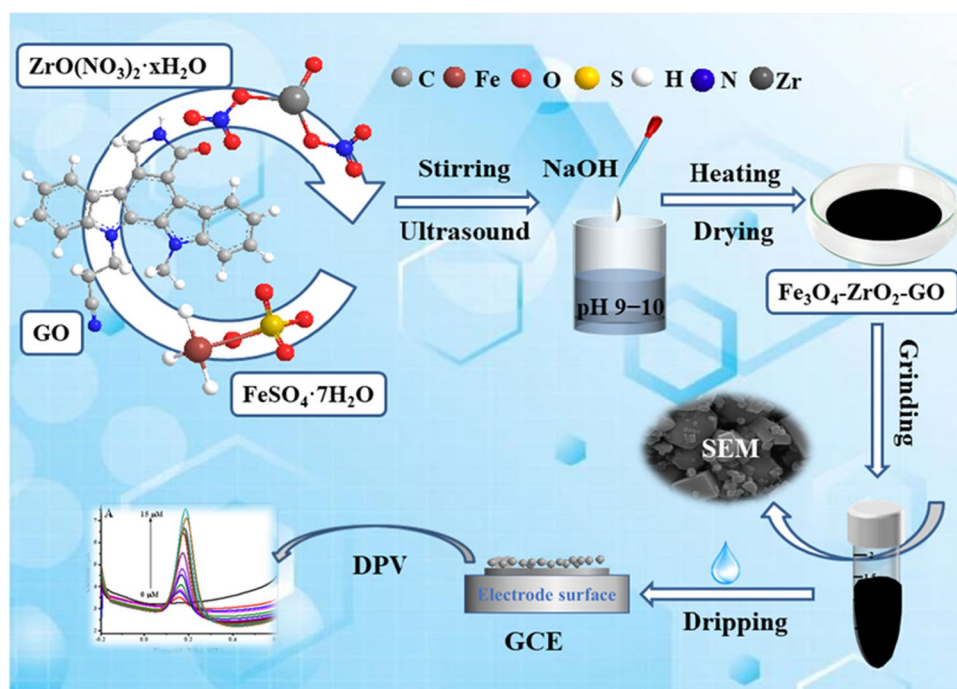
Synthesis of Fe₃O₄- ZrO₂-GO

0.10 g Fe₃O₄-GO was added to 20 mL water for ultrasonic dispersion of 30 min, and 0.0999 g zirconium nitrate hydrate was added to the above suspension under agitation. The pH value of the solution was adjusted to $9-10$ with 0.50 mol L^{-1} NaOH solution, and the mixed solution was moved into the autoclave, which was heated at 180 ℃ for 8 h. The resulting sample was washed with ethanol and water respectively to pH 7 and dried at 60 ℃ for 12 h, and the final product (Fe₃O₄- ZrO₂-GO) was obtained.

Electrochemical measurements

The type, parameters of three-electrode system, measurement method, and preparation of dispersion liquid for electrochemical measurement were provided in our previous work [39], which will not be described here. The schematic representation of the fabrication process for Fe₃O₄- ZrO₂-GO/GCE and main test methods to DA are briefly illustrated in Scheme 1.

Results and discussion

Characterizations

XRD and FTIR analysis

Figure 1 shows the XRD patterns of GO, ZrO₂, Fe₃O₄, and Fe₃O₄-ZrO₂-GO. In Fig. 1A, the strong diffraction peaks at 2θ of 30.167°, 35.307°, 49.785°, and 59.725° correspond, respectively, to (111), (200), (202), and (311) crystal planes of ZrO₂ (JCPDS NO.37–1484). In Fig. 1B, the diffraction peaks at 2θ of 18.988°, 31.249°, 36.820°, 38.524°, 44.762°, 53.412°, 56.959°, 62.561°, and 74.460° are, respectively, indexed to (111), (220), (311), (222), (400), (422), (511), (440), and (533) crystal planes of Fe₃O₄ (JCPDS NO.26–1136). The sharp peak indicates it is with good crystallinity. In Fig. 1C, the diffraction peak at 2θ of 10.615° is ascribed to the (001) crystal planes of GO (JCPDS NO.44–0558), which can also be observed on the XRD pattern of Fe₃O₄-ZrO₂-GO. Meanwhile, a set of peaks similar to Fe₃O₄ and ZrO₂ are clearly visible on the ternary composites, indicating that Fe₃O₄ and ZrO₂ are successfully loaded on the GO surface with high purity.

Figure 1D shows the FTIR of GO, ZrO₂, Fe₃O₄, and Fe₃O₄-ZrO₂-GO. For all the FTIR curves, the absorption bands around 3400 cm^{-1} are attributes to $-OH$ asymmetric stretching vibration of $C-OH$ groups and/or water between the layers of GO, the band near 2356 cm^{-1} is ascribed to atmospheric CO_2. For GO, the peak appeared at 1700 cm^{-1} is due to $C=O$ stretching vibrations in carboxylic acid and carbonyl groups, and the peak at 1541 cm^{-1} belonged to the vibration band of unoxidized graphite skeleton $C=C$. The absorption bands at 1623 and 1400 cm^{-1} confirm the presence of vibrational modes of C–C aromatics and C–O carboxyl groups, respectively. The peak at 1045 cm^{-1} is assigned to C–O alkoxy group [40]. The vibrations around 553 cm^{-1} and 709 cm^{-1} arise from the Zr–O vibrations of the tetragonal ZrO₂. A sharp band around 752 cm^{-1} is characteristic for monoclinic
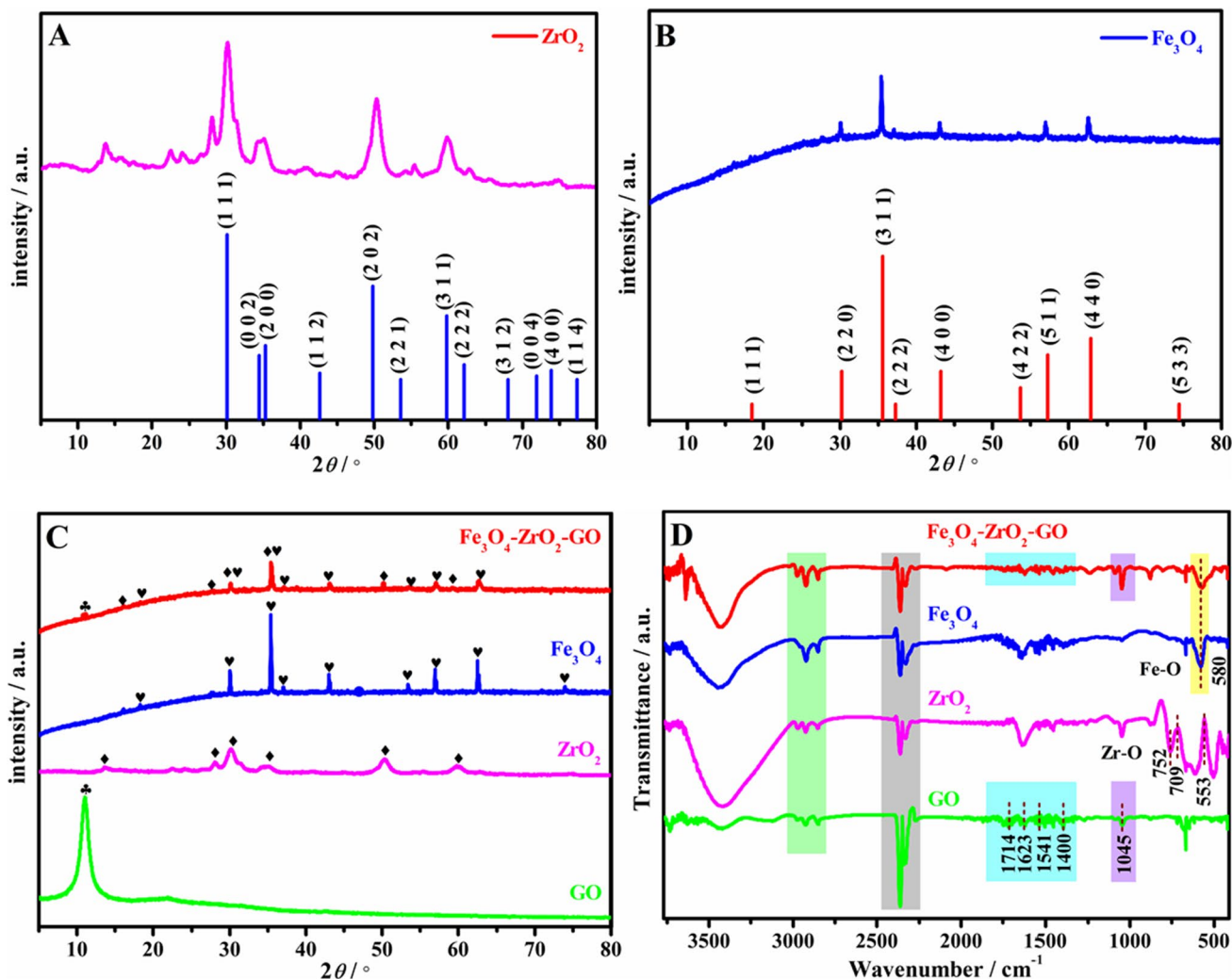
Fig. 1 XRD patterns of **A** ZrO_2, **B** Fe_3O_4, **C** GO, ZrO_2, Fe_3O_4, and Fe_3O_4-ZrO_2-GO, **D** FTIR spectra of GO, ZrO_2, Fe_3O_4, and Fe_3O_4-ZrO_2-GO

ZrO_2. [41] As for Fe_3O_4, the characteristic absorption band near 580 cm^{-1} is ascribed to Fe–O stretching vibration of the magnetite phase [42]. Likewise, the characteristic peaks of Fe–O, Zr–O and GO appear in the infrared spectrum of Fe_3O_4-ZrO_2-GO. Combined with XRD results, FTIR further verifies the successful preparation of Fe_3O_4-ZrO_2-GO.

SEM images

SEM images of different materials are shown in Fig. 2. It can be observed from Fig. 2A that GO presents a typical folded layered structure. The image of ZrO_2 shown in Fig. 2B is porcelain flake with uniform distribution and relatively smooth surface when viewed at magnification scale. The flake thickness is about a few nanometers. In Fig. 2C, Fe_3O_4 shows a cube particle with uniform particle size. The particle sizes range from a few hundred nanometers to a few microns.

In Fig. 2D, the morphology of Fe_3O_4-ZrO_2-GO composite presents irregular block and flake with a small amount of grain agglomerations, which can be observed more clearly in the enlarged image (Fig. 2E). Figure 2F is the EDS spectra of Fe_3O_4-ZrO_2-GO. The weight ratios of C, O, Fe, and Zr in ternary materials are 47.41%, 46.37%, 5.36%, and 0.86%, which further verifies the coexistence of Fe_3O_4, ZrO_2, and GO. In addition, element mapping analysis was performed for Fe_3O_4-ZrO_2-GO. It can be found from Fig. 2G – J the ternary composite is composed of C, O, Zr, and Fe elements, and the distribution of elements is more uniform.

XPS analysis

The elemental composition and oxidation state of Fe_3O_4-ZrO_2-GO ternary composites were characterized by XPS. The survey spectrum in Fig. 3A confirms the coexistence of Zr, C, O, and Fe elements in Fe_3O_4-ZrO_2-GO. The

Fig. 2 SEM images of **A** GO, **B** ZrO_2, **C** Fe_3O_4, and **D, E** Fe_3O_4-ZrO_2-GO. **F** EDS spectra of Fe_3O_4- ZrO_2-GO. Element mapping of **G** C, **H** O, **I** Zr, and **J** Fe
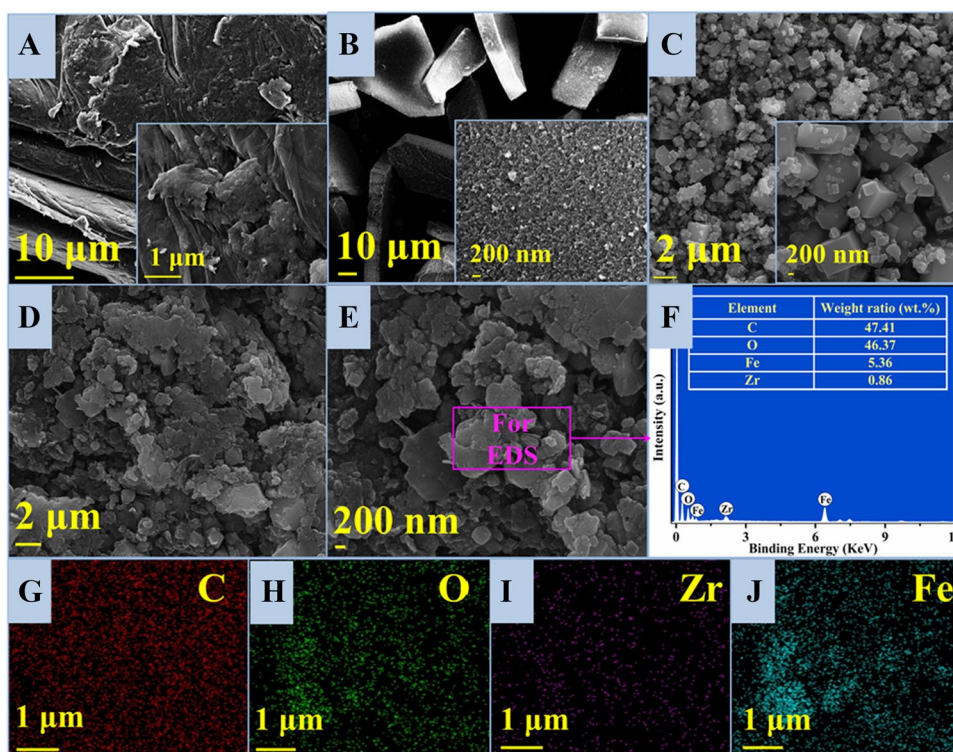
high-resolution XPS spectrum of Zr 3d in Fig. 3B shows the two spin orbit of Zr $3d_{5/2}$ (182.48 eV) and Zr $3d_{3/2}$ (184.78 eV), which are consistent with the typical Zr^{4+} ions [43–45]. In Fig. 3C, four peaks of C 1 s are assigned to C−C/C=C (284.18 eV), C−O (285.28 eV), C=O (287.58 eV), and O−C=O (289.38 eV) respectively, which is in agreement with XPS spectra of GO in literature [46, 47]. In Fig. 3D, the O1s region is deconvoluted into three spectral peaks. The most intense peak at 529.78 eV is due to the lattice oxygen in the metal oxide. The peak near 531.18 eV is ascribed to the carbonyl (C=O), and the relatively small peak around 532.68 eV is attributed to C−O [35, 48]. Fig. 3E shows the XPS spectrum of Fe 2p. Two strong characteristic peaks appeared around 710 and 724 eV are assigned to Fe $2p_{3/2}$ and Fe $2p_{1/2}$, which can be divided into two sub-peaks with binding energies of 709.88, 711.18 eV, and 724.18, 725.78 eV, corresponding to Fe^{2+} and Fe^{3+}, respectively. Two accompanied satellite (Sat.) peaks (715.48, 732.48 eV) indicate the presence of Fe_3O_4 in the composite [49–, 50–54]. In addition, the ratios of Fe^{2+} to Fe^{3+} for Fe $2p_{3/2}$ and Fe $2p_{1/2}$ are both less than 1, which means that during the formation of Fe_3O_4-ZrO_2-GO, part of Fe^{2+} ions are converted into Fe^{3+} ions. [35, 55, 56]

Optimization of test conditions

Optimization of pH

CV was used to investigate the influence of pH between 5.0 and 9.0 in the determination of DA by Fe_3O_4-ZrO_2-GO

modified GCE (Fig. S1A). It is obvious that with the increase of pH, the peak current reaches the maximum value at pH 7.0, and the peak shape is obvious, which has a better response to DA. Considering the sensitivity of physiological environment, pH 7.0 was selected for further experiments.

Optimization of the ratio of materials

The properties of GCE modified by composite materials with five weight ratios in 0.2 M PBS solution (pH 7.0) containing 5 µM DA were also investigated (Fig. S1B). It can be observed that the composite material has a certain response to DA, and the peak current varies with the different proportions. By contrast, when the weight ratio of Fe_3O_4-GO /ZrO_2 is 1:1, the response signal is the strongest, and the obvious redox peak can be observed. This phenomenon may be caused by the fact that when the weight ratio of Fe_3O_4-GO /ZrO_2 is 2:1 or 1.3:1, the dosage of ZrO_2 is too small, and its excellent performance is unconspicuous, and the synergy between the three substances cannot be fully reflected, resulting in not much increase of the active site of the hybrid. However, when their weight ratio is 1:1.25 or 1:1.5, excessive ZrO_2 will lead to the degradation of electrocatalytic performance due to the decrease of electrical conductivity. Therefore, the weight ratio of Fe_3O_4-GO /ZrO_2 of 1:1 was selected for the next experiment.
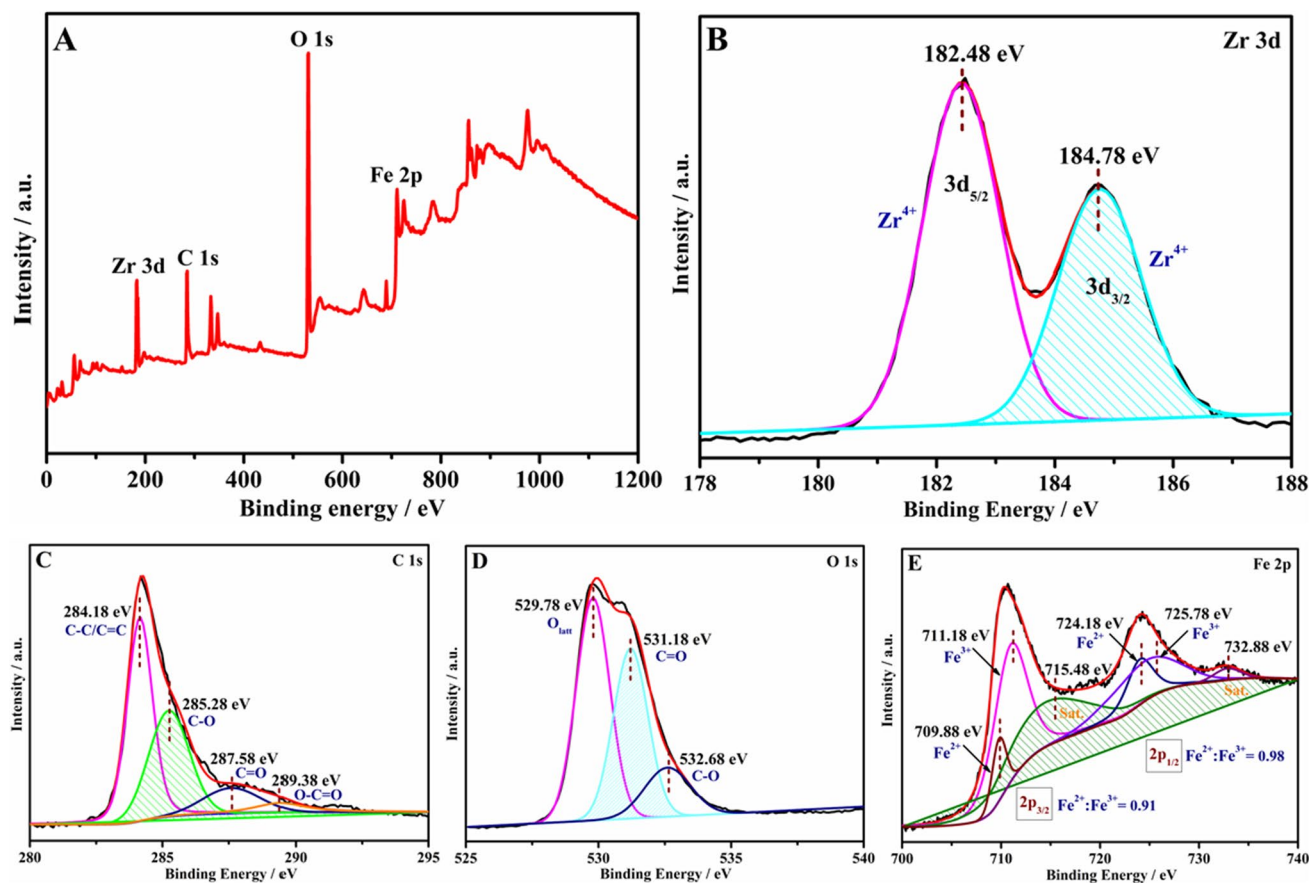
Fig. 3 XPS spectra of **A** survey spectrum, **B** Zr 3d, **C** C 1 s, **D** O 1 s, and **E** Fe 2p

Optimization of the amount of the target material on the electrode surface

The electrochemical behavior of Fe_3O_4-ZrO_2-GO composites with different contents on the electrode surface was studied by DPV (Fig. S1C). Keeping 5 μL of modified ink on the electrode surface every time, and the optimal content of target substance in the electrode modified ink was explored. It can be noted that the DPV signal changes with the amount. When the target substance is 5.0 mg, the response to DA is the strongest. Therefore, 5.0 mg was selected for further exploration.

Electrochemical characterization

CV analysis

CV curves of GO, ZrO_2, Fe_3O_4, and Fe_3O_4-ZrO_2-GO modified GCE were tested in 0.1 M KCl solution containing 5 mM $[Fe(CN)_6]^{3-/4-}$ at the scan rate of 100 mVs^{-1} (Fig. S2). It can be noticed that CV shows good reversible wave, which is caused by the redox reaction of potassium ferricyanide on the electrode surface. The peak current of the

Fe_3O_4-ZrO_2-GO composite is significantly increased compared with that of GO, ZrO_2, and Fe_3O_4. The relevant data are listed in Table 1.

As shown in Table 1, the potential difference between two peaks ($\Delta E_p = E_{\text{anodic-peak}} - E_{\text{cathodic-peak}}$) of the Fe_3O_4-ZrO_2-GO modified GCE is 0.142 mV, which is smaller than that of other test materials, indicating Fe_3O_4-ZrO_2-GO/GCE shows better electrochemical performance. Moreover, the peak current of the Fe_3O_4-ZrO_2-GO composite (143.6 μA) is the highest among all electrode materials. For reversible CV reactions, the peak current can be used to calculate the electrochemical active surface area of the modified electrode on basis of Randles–Sevcik equation.

$$I_p = 2.69 \times 10^5 A D^{1/2} n^{3/2} v^{1/2} C \tag{1}$$

where I_p, A, D, n, ν, and C represent the peak current (A), the surface area of the electrode (m^2), the diffusion coefficient ($D = 7.6 \times 10^{-3}$ cm^2 s^{-1}), the number of electrons in the electrode reaction ($n = 1$), the scanning rate ($\nu = 0.1$ V s^{-1}), and the concentration of $[Fe(CN)_6]^{3-/4-}$ ($C = 5 \times 10^{-3}$ M), respectively. [57] Obviously, compared with other modified electrodes (GO, 0.01 cm^2; ZrO_2, 0.09 cm^2; Fe_3O_4, 0. 13

Table 1 ΔE_p, I_p and electroactive active surface areas of different modified GCE

Materials	$E_{\text{anodic-peak}}$	$E_{\text{cathodic-peak}}$	ΔE_p/mV	I_p (µA)	Electroactive surface area (cm^2)
GO/GCE	0.288	0.146	0.142	9.5	0.01
Fe$_3$O$_4$/GCE	0.290	0.117	0.173	99.5	0.13
ZrO$_2$/GCE	0.287	0.123	0.164	71.6	0.09
Fe$_3$O$_4$-ZrO$_2$-GO/GCE	0.270	0.128	0.142	143.6	0.18

cm^2), Fe$_3$O$_4$-ZrO$_2$-GO/GCE has higher electroactive surface area (0.18 cm^2), indicating that Fe$_3$O$_4$-ZrO$_2$-GO has good conductivity, which promotes the electron transfer of potassium ferricyanide on the electrode surface, and thus speeding up the reaction.

CV response to DA

In addition, CV method was also employed to investigate the electrochemical response of GO, Fe$_3$O$_4$, ZrO$_2$, and Fe$_3$O$_4$-ZrO$_2$-GO modified GCE towards DA. Figure 4A − D shows the CVs of GO, Fe$_3$O$_4$, ZrO$_2$, and Fe$_3$O$_4$-ZrO$_2$-GO modified GCE in 0.2 M phosphate buffer solution (PBS, pH7.0) with and without DA (5 µM). All the modified GCEs have a certain response to DA. In contrast, the single GO/GCE, ZrO$_2$/GCE, and Fe$_3$O$_4$/GCE exhibit weak response to DA, while the ternary Fe$_3$O$_4$-ZrO$_2$-GO/GCE has an obvious peak for DA detection. Figure 4E is the CV comparison of different materials modified GCE in 0.2 M PBS containing 5 µM DA. Compared with other related single materials modified GCE, Fe$_3$O$_4$-ZrO$_2$-GO/GCE presents a pair of distinct redox peaks, which is consistent with the peak position of DA in literature [58, 59]. The oxidation mechanism of DA is expressed in Scheme 2. [59] Furthermore, the corresponding CV areas are presented in Fig. 4F. The results show that Fe$_3$O$_4$-ZrO$_2$-GO/GCE has the largest CV area, indicating it has a good signal for DA detection.

EIS analysis

Figure 5 shows the electrochemical impedance spectroscopy (EIS) plot of different materials in 5 mM [Fe(CN)$_6$]$^{3-/4-}$ solution. Inset is an equivalent circuit, where, R_s, R_{ct}, and Z_w represent electrolyte resistance, charge transfer resistance, and Warburg impedance, respectively. The R_{ct} value of Fe$_3$O$_4$-ZrO$_2$-GO modified electrode (14.11 Ω) is lower than that of GO (29.28 Ω), Fe$_3$O$_4$ (20.83 Ω), ZrO$_2$ (14.88 Ω), indicating that Fe$_3$O$_4$-ZrO$_2$-GO has good electron transport capability.

Electrochemical kinetics

Figure S3A shows the CV response of Fe$_3$O$_4$-ZrO$_2$-GO modified GCE to DA at the different scan rates (50–300 mVs^{-1}). As the scan rate increases from 50 to 300 mVs^{-1}, the peak current also increases and the peak potential has slightly positive or negative shift. It can be observed from Fig. S3B that both oxidation peak current and reduction peak current are proportional to the square root of scanning rates, and the linear regression equation is expressed as $I_{pa} = 6.91\nu^{1/2} - 18.29$ ($R^2 = 0.99311$), and $I_{pc} = -8.11\nu^{1/2} + 25.92$ ($R^2 = 0.99785$), which further verifies that the reaction to DA is quasi-reversible, and the electrocatalytic oxidation process of DA on Fe$_3$O$_4$-ZrO$_2$-GO modified GCE surface is a typical diffusion-control process. [60, 61]

Electrochemical performance of Fe$_3$O$_4$-ZrO$_2$-GO composite modified GCE

Linear range and detection limit of DA

Differential pulse voltammetry (DPV) has been used to study the electrochemical performance of the as-prepared electrode materials towards DA. DPV of Fe$_3$O$_4$-ZrO$_2$-GO composite modified GCE was detected in 0.20 M PBS (pH7.0) containing different concentrations of DA. As shown in Fig. 6A, with the increasing concentration of DA, the oxidation peak current also increases, and within the concentration range of 0.5 − 15 µM (0, 5, 10, 20, 40, 60, 100, 150, 200, 300 µM), there is a linear relationship with the oxidation peak current of DA detection (Fig. 6B). Its linear regression equation is $Y = 0.2554x + 0.0056$ ($R^2 = 0.9804$), and the sensitivity (S) is 3.649 µA µm^{-1} cm^{-2}. The detection limit is 0.1562 µM calculated according to LOD $= 3S_b/S$, where S_b is the standard deviation of five blank samples.

In addition, the results of Fe$_3$O$_4$-ZrO$_2$-GO/GCE for DA detection were compared with those of reported modified electrodes (Table 2). The results suggest the Fe$_3$O$_4$-ZrO$_2$-GO/GCE exhibits wide linear range and a lower detection limit for DA. It is speculated that the excellent performances are mainly attributed to the good sensitivity of
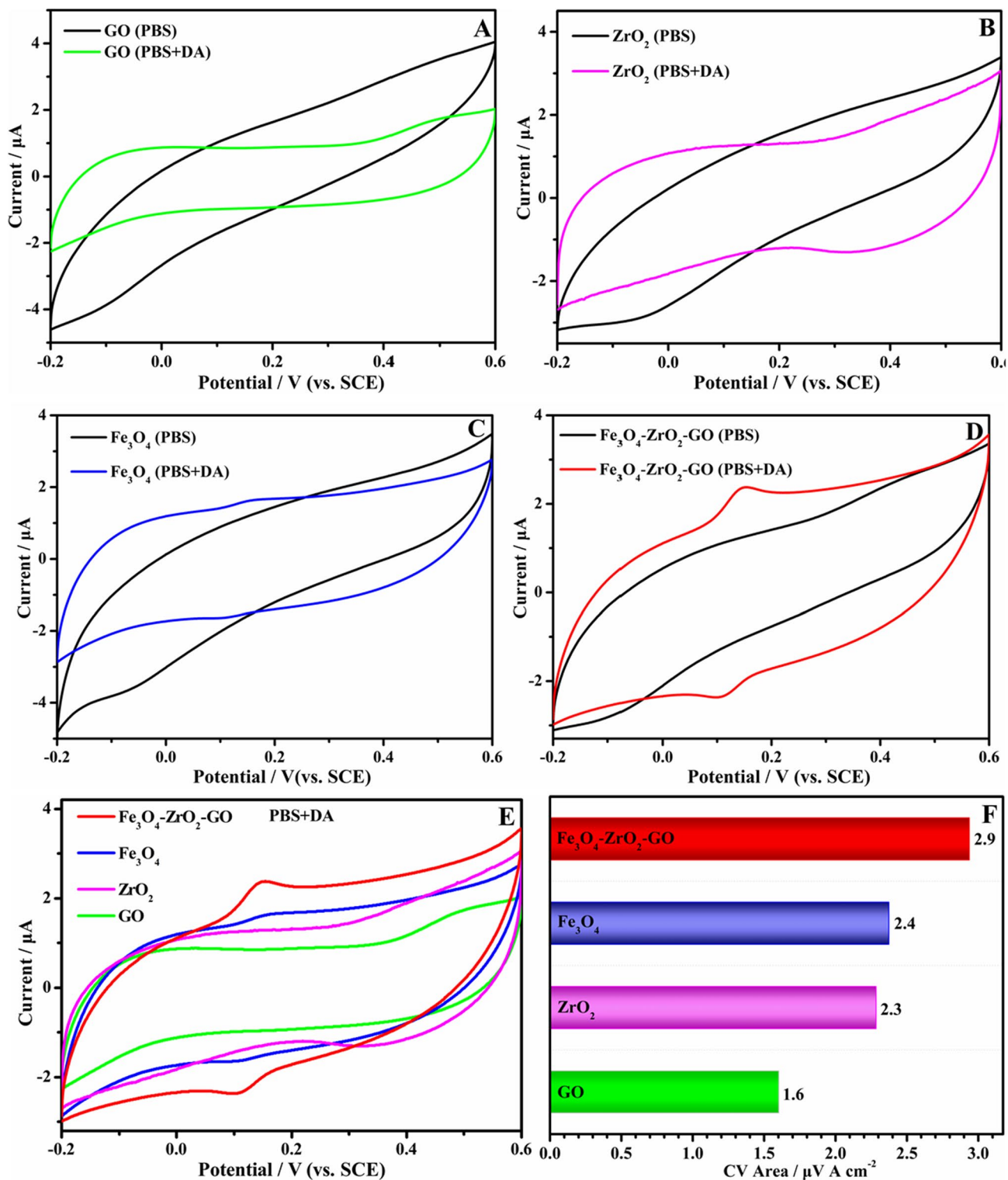
Fig. 4 CV curves of **A** GO, **B** ZrO₂, **C** Fe₃O₄, and **D** Fe₃O₄-ZrO₂-GO modified GCE in 0.2 M PBS electrolyte (pH7.0) with and without 5 μMDA solution. **E** CV combination pattern of GO, ZrO₂, Fe₃O₄, and Fe₃O₄-ZrO₂-GO modified GCE in 0.2 M PBS electrolyte (pH7.0) containing 5 μM DA solution. **F** Histogram of corresponding CV area

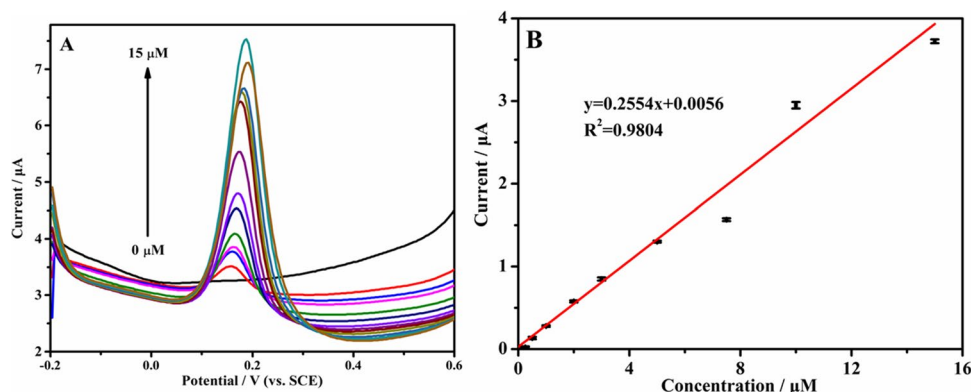**Scheme 2** Oxidation mechanism of DA at Fe_3O_4-ZrO_2-GO modified GCE

$$\text{Dopamine} \quad \xrightleftharpoons{-2H^+-2e^-} \quad \text{Dopaminequinone}$$
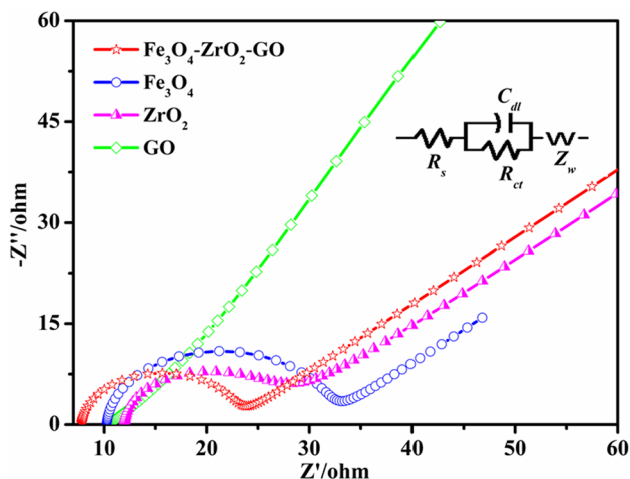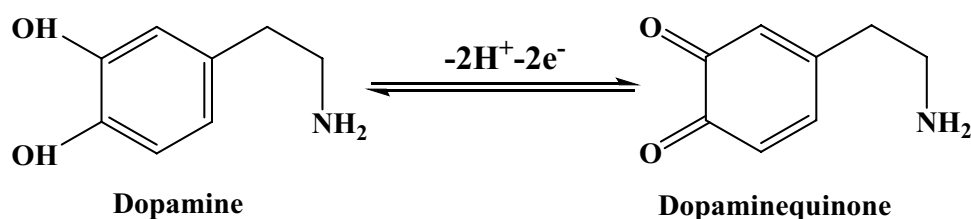
Fig. 5 Nyquist plot of GO, ZrO_2, Fe_3O_4, and Fe_3O_4-ZrO_2-GO modified GCE. (Inset) equivalent circuit

the metal oxides, the larger specific surface area, and higher electrical conductivity of GO, as well as the synergistic amplification effect brought from Fe_3O_4, ZrO_2, and GO.

Anti-interference

Figure 7A shows the anti-interference test of Fe_3O_4-ZrO_2-GO composite by DPV method. Then, 100 μL of 0.25 mM dopamine (DA) was added into 10 mL of 0.20 M PBS solution (pH 7.0) for the DPV test. After that, the same concentration of uric acid (UA), D(+) -glucose (Glu), L-Cystine, L-Cysteine, and ascorbic acid (AA) were successively added into the above solution to repeat the operation, and

the current changes of the whole process were observed. The change rates of the corresponding peak current are shown in Fig. 7B. The influence of all potential interfering substances on the current is less than 5%, indicating that the Fe_3O_4-ZrO_2-GO composite still has good selectivity in the presence of the above interfering substances.

Stability and reproducibility

Fe_3O_4-ZrO_2-GO composite modified GCE was used as an electrochemical sensor, and 5 μM dopamine was detected by CV in 0.20 M PBS electrolyte (pH7.0) for 5 consecutive days. Figure 8A is the CV curves of DA detection with composite modified electrode during these 5 days. It can be noticed that the peak current decreases slightly with the increase of days. The relationship between the peak current of DA oxidation and time can be more clearly showed in Fig. 8B. The peak current on the last day does not decrease much compared to the peak current on the first day, and the peak current on 5th day is 91.18% of that on 1st day, which proves that the Fe_3O_4-ZrO_2-GO/GCE has good stability in DA detection.

Reproducibility was measured as follows: Five different Fe_3O_4-ZrO_2-GO composite modified electrodes were selected and 5 μM DA was detected by CV method in 0.20 M PBS electrolyte (pH7.0). The results are shown in Fig. 9A. When different electrodes were used for detection, the oxidation peak current of DA does not change much. As shown in Fig. 9B, the relative standard deviation for oxidation peak current is 3.76%, implying that the Fe_3O_4-ZrO_2-GO/ GCE has good reproducibility in DA detection.

Fig. 6 A DPV curves of Fe_3O_4-ZrO_2-GO/GCE in 0.20 M PBS (pH = 7.0) containing different concentrations of DA (0.5 − 15 μM). **B** Relation plot of oxidation peak current versus concentration of DA

Table 2 Comparison of electrochemical detection for DA on Fe_3O_4-ZrO_2-GO/GCE with recent reported modified electrodes

Electrode materials	Methods	Linear range (μM)	Detection limit (μM)	References
GO	DPV	1 – 15	0.27	[62]
GO/TmPO$_4$	DPV	2 – 10	0.785	[63]
GO-PANI /GCE	DPV	2 – 14	0.5	[64]
AGONF/CPE	CV	2 – 7	0.84	[65]
Chite-GR/GCE	DPV	1 – 24	1.0	[66]
CCE/Fc	SWV	1 – 2.5	0.45	[67]
PSA/GCE	DPV	1 – 6	0.33	[68]
PEDOT/Pd composite	DPV	0.5 – 1	0.5	[69]
Fe_3O_4-ZrO_2-GO/GCE	DPV	0.5 – 15	0.1562	This work

GO-PANI graphene oxide / polyaniline, *AGONF/CPE* alanine functionalized GO nanoflakes / carbon paste electrode, *Chite-GR* chitosan graphene, *CCE/Fc* a carbon ceramic electrode modified with ferrocenecarboxylic acid, *SWV* square wave voltammetry, *PSA/GCE* poly(sulfosalicylic acid) modified GC electrode, *PEDOT* poly (3,4-ethylenedioxythiophene)

Fig. 7 **A** DPV curve for DA and other interferences at Fe_3O_4-ZrO_2-GO modified GCE. **B** Change rate of peak current
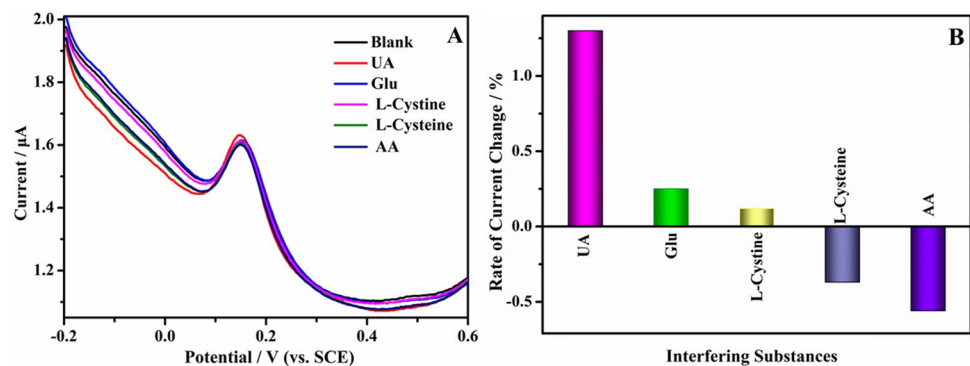
Fig. 8 Stability test of Fe_3O_4-ZrO_2-GO/GCE: **A** CV. **B** Histogram of peak current
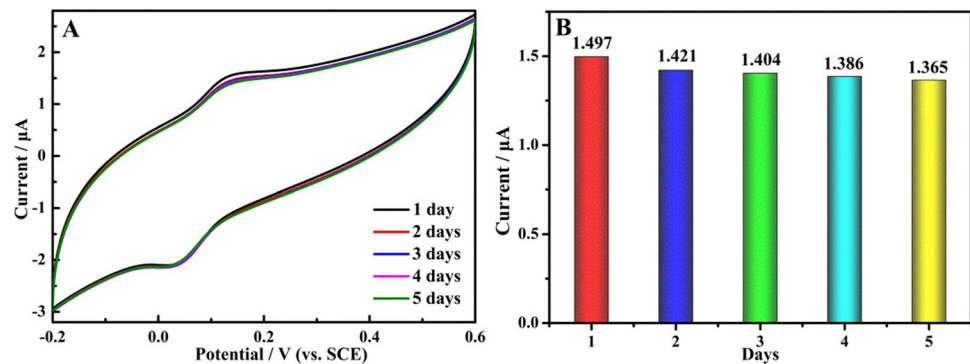
Test of real samples

In order to verify the reliability of the method for the DA detection, the as-prepared Fe_3O_4-ZrO_2-GO modified GCE was applied to determine DA in real human serum by standard addition method. All serum samples were diluted 10 times with PBS (pH7.0). Each sample passed 5 parallel DPV tests. To evaluate the accuracy of the method, a standard DA solution with a known concentration (1.0 mM) was added to the electrolyte. The test results listed in Table 3 show that the Fe_3O_4-ZrO_2-GO/GCE sensor has satisfactory recovery rate within the range of 98.8 – 102.0% and good relative standard deviation (RSD) (0.34 – 0.36%), and so it has the potential of practical application.

Fig. 9 Reproducibility test of Fe_3O_4-ZrO_2-GO modified electrodes: **A** CV. **B** Histogram of peak current
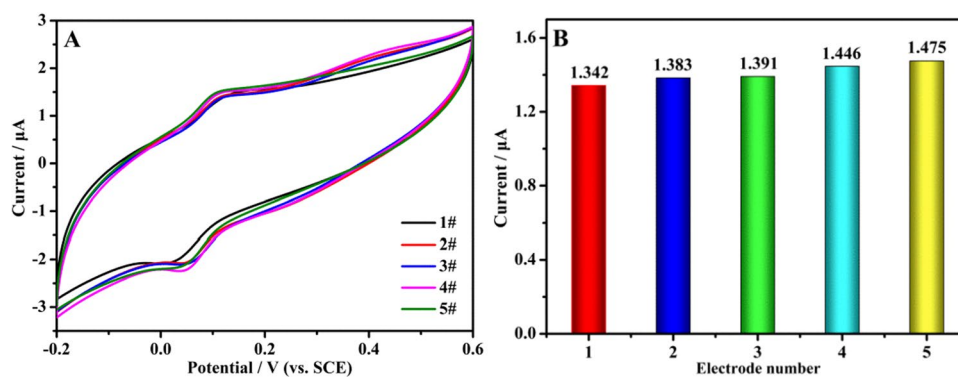
Table 3 Detection of DA in human serum

Sample	Added (µM)	Found (µM)	Recovery (%)	RSD (%)
Serum 1	10	9.88	98.8	0.35
Serum 2	5	4.85	97.0	0.34
Serum 3	10	10.2	102.0	0.36

Conclusion

In this work, a novel electrochemical sensor based on Fe_3O_4-ZrO_2-GO composite was developed for the detection of dopamine. Among which, GO is used as the substrate and loaded with two metal oxides. It not only enhances the conductivity, but also, together with ZrO_2, weakens the accumulation of Fe_3O_4, exposing more active sites of composite. The sensor based on Fe_3O_4-ZrO_2-GO/GCE exhibits excellent electrocatalytic performance for DA detection. In the concentration range of $0.5-15$ µM, its sensitivity is 3.649 µA µm^{-1} cm^{-2}, the detection limit is 0.1562 µM. Additionally, Fe_3O_4-ZrO_2-GO/GCE also shows good anti-interference capability, stability, and reproducibility, and it was successfully used in the determination of DA in human serum. This study is expected to open up a new way for the construction of sensitive sensor based on bimetallic oxides.

Declarations

Competing interests The authors declare no competing interests.

References

1. Wang L, Yang R, Qu L, Harrington PB (2020) Electrostatic repulsion strategy for high-sensitive and selective determination of dopamine in the presence of uric acid and ascorbic acid. Talanta 210:120626
2. Dong XX, Xu CX, Lu S, Wang R, Shi ZL, Cui QN, You TY (2021) ZIF-8 coupling with reduced graphene oxide to enhance the electrochemical sensing of dopamine. J Electrochem Soc 168:116517
3. Ma L, Zhao T, Zhang P, Liu M, Shi H, Kang W (2020) Determination of monoamine neurotransmitters and metabolites by high-performance liquid chromatography based on Ag (III) complex chemiluminescence detection. Anal Biochem 593:113594
4. Poh EZ, Hahne D, Moretti J, Harvey AR, Clarke MW, Rodger J (2019) Simultaneous quantification of dopamine, serotonin, their metabolites and amino acids by LC-MS/MS in mouse brain following repetitive transcranial magnetic stimulation. Neurochem Int 131:104546
5. Ma S, Xu Z, Ren J (2019) Analysis of neurochemicals by capillary electrophoresis in athletes' urine and a pilot study of their changes responding to sport fatigue. Anal Methods 11:2712
6. Ling Y, Wang L, Zhang XY, Wang XH, Zhou J, Sun Z, Li NB, Luo HQ (2020) Ratiometric fluorescence detection of dopamine based on effect of ligand on the emission of Ag nanoclusters and aggregation-induced emission enhancement. Sensor Actuat B-Chem 310:127858
7. Zhang RX, Fan ZF (2020) Nitrogen-doped carbon quantum dots as a "turn off-on" fluorescence sensor based on the redox reaction mechanism for the sensitive detection of dopamine and alpha lipoic acid. J Photoch Photobio A 392:112438
8. Olmo F, Garoz-Ruiz J, Colina A, Heras A (2020) Derivative UV/Vis spectroelectrochemistry in a thin-layer regime: deconvolution and simultaneous quantification of ascorbic acid, dopamine and uric acid. Anal Bioanal Chem 412:6329–6339
9. Li C, Zhang YY, Li CY, Wan QJ, Ke Q, Yang NJ (2020) Tailoring the CeO$_2$ morphology and its electrochemical reactivity for highly sensitive and selective determination of dopamine and epinephrine. Microchim Acta 187(2):143

10. Zou J, Guan JF, Zhao GQ, Jiang XY, Liu YP, Yu JG, Li WJ (2021) Construction of a highly sensitive signal electrochemical sensor based on self-assembled cobalt oxide-hydroxylated single-walled carbon nanotubes composite for detection of dopamine in bovine serum samples. J Environ Chem Eng 9:105831

11. Kumar RS, Govindan K, Ramakrishnan S, Kim AR, Kim JS, Yoo DJ (2021) Fe_3O_4 nanorods decorated on polypyrrole/reduced graphene oxide for electrochemical detection of dopamine and photocatalytic degradation of acetaminophen. Appl Surf Sci 556:149765

12. Yar A, Krishnan SG, Dennis JO, Yasin A, Khalid M, Yang CC, Jose R (2022) Metal oxide nanotubes via electrodeposition for battery-electrochemical capacitor hybrid device. Synth Met 284:116991

13. Li WJ, Nagashima K, Hosomi T, Liu JY, Takahashi T, Zhang GZ, Tanaka W, Kanai M, Yanagida T (2022) Core-shell metal oxide nanowire array to analyze adsorption behaviors of volatile molecules. Chem Lett 51(4):424–427

14. Selvi SV, Nataraj N, Chen SM (2020) The electro-catalytic activity of nanosphere strontium doped zinc oxide with rGO layers screen-printed carbon electrode for the sensing of chloramphenicol. Microchem J 159:105580

15. Ayaz S, Karakaya S, Emir G, Usaklıgil N, Dilgin DG, Dilgin Y (2022) Flow-injection amperometric determination of Glucose using nickel oxide-cobalt (II, III) oxide and nickel oxide-copper nanoparticle modified pencil graphite electrodes. Anal Lett 55(13):2046–2057

16. Xu YL, Shi XF, Hua R, Zhang R, Yao YJ, Zhao B, Liu T, Zheng JZ, Lu G (2020) Remarkably catalytic activity in reduction of 4-nitrophenol and methylene blue by Fe_3O_4@COF supported noble metal nanoparticles. Appl Catal B-Environ 260:118142

17. Liu YX, Zhu WJ, Wu D, Wei Q (2015) Electrochemical determination of dopamine in the presence of uric acid using palladium-loaded mesoporous Fe_3O_4 nanoparticles. Measurement 60:1–5

18. Rejinold NS, Thomas RG, Muthiah M, Lee HJ, Jeong YY, Park I, Jayakumar R (2016) Breast tumor targetable Fe_3O_4 embedded thermo-responsive nanoparticles for radiofrequency assisted drug delivery. Nanotechnology 12:43–55

19. Jamil S, Janjua MRSA (2017) Synthetic study and merits of Fe_3O_4 nanoparticles as emerging material. J Clust Sci 28:2369–2400

20. Liu Y, Zhou J, Gong J, Wu WP, Bao N, Pan ZQ, Gu HY (2013) The investigation of electrochemical properties for Fe_3O_4@Pt nanocomposites and an enhancement sensing for nitrite. Electrochim Acta 111:876–887

21. Zeng H, Li J, Liu JP, Wang ZL, Sun S (2002) Exchange-coupled nanocomposite magnets by nanoparticle self-assembly. Nature 420:395–398

22. Chen XJ, Zhu JW, Chen ZX, Xu CB, Wang Y, Yao C (2011) A novel bienzyme glucose biosensor based on three-layer Au-Fe_3O_4@SiO_2 magnetic nanocomposite. Actuat B Chem 159:220–228

23. Arvand M, Hassannezhad M (2014) Magnetic core–shell Fe_3O_4@SiO_2/MWCNT nanocomposite modified carbon paste electrode for amplified electrochemical sensing of uric acid. Mater Sci Eng C 36:160–167

24. Feng TT, Qiao XW, Wang HN, Sun Z, Hong CL (2016) A sandwich-type electrochemical immunosensor for carcinoembryonic antigen based on signal amplification strategy of optimized ferrocene functionalized Fe_3O_4@SiO_2 as labels. Biosens Bioelectron 79:48–54

25. Han SY, Du TY, Lai LM, Jiang XR, Cheng CS, Jiang H, Wang XM (2016) Highly sensitive biosensor based on the synergistic effect of Fe_3O_4-Co_3O_4 bimetallic oxides and graphene. RSC Adv 6:82033

26. Starschich S, Schenk T, Schroeder U, Boettger U (2017) Ferroelectric and piezoelectric properties of $Hf_{1-x}Zr_xO_2$ and pure ZrO_2 films. Appl Phys Lett 110:182905

27. Huang CY, Chen YL (2016) Design and impact resistant analysis of functionally graded Al_2O_3–ZrO_2 ceramic composite. Mater Design 91:294–305

28. Wu S, Zhang DT, Yue M, Wang YQ, Shang ZF, Wu D, Liang J (2019) In-situ observation of magnetization reversal process of Sm(Co, Cu, Fe, Zr)z magnets with different Fe contents. Rare Met 39:250–255

29. Cui GQ, Zhang X, Wang H, Li ZY, Wang WL, Yu Q, Zheng LR, Wang YD, Zhu J, Wei M (2020) ZrO_{2-x} modified Cu nanocatalysts with synergistic catalysis towards carbonoxygen bond hydrogenation. Appl Catal B-Environ 280:119406

30. Lou CM, Li ZS, Yang C, Liu XH, Zheng W, Zhang J (2021) Rational design of ordered porous SnO_2/ZrO_2 thin films for fast and selective triethylamine detection with humidity resistance. Sensor Actuat B Chem 333:129572

31. Koichi S, Hotaka U, Takaharu M, Ken W, Kengo S (2019) Oxygen adsorption on ZrO_2-loaded SnO_2 gas sensors in humid atmosphere. J Mater Sci 54:3135–3143

32. Dreye DR, Park S, Bielawski CM, Ruoff RS (2010) The Chemistry of Graphene Oxide. Chem Soc Rev 39:228–240

33. Chen D, Feng HB, Li JH (2012) Graphene oxide: preparation functionalization, and electrochemical applications. Chem Rev 112:6027–6053

34. Wang Y, Li ZH, Wang J, Li JG, Lin YH (2011) Graphene and graphene oxide: biofunctionalization and applications in biotechnology. Trends Biotechnol 29:205–212

35. Majumder S, Sardar M, Satpati B, Kumar S, Banerjee S (2018) Magnetization enhancement of Fe_3O_4 by attaching onto graphene oxide: an interfacial effect. J Phys Chem C 122:21356–21365

36. Pei S, Cheng HM (2012) The reduction of graphene oxide. Carbon 50:3210–3228

37. Stebunov YV, Aftenieva OA, Arsenin AV, Volkov VS (2015) Highly sensitive and selective sensor chips with graphene-oxide linking layer. ACS Appl Mater Inter 7:21727–21734

38. Marcano DC, Kosynkin DV, Berlin JM, Sinitskii A, Sun ZZ, Slesarev AS, Alemany LB, Lu W, Tour JM (2010) Improved synthesis of graphene oxide. ACS Nano 4:4806

39. Wang HY, Zhu SC, Liu CY, Gu LY, Chang JN, Xie AJ, Luo SP (2021) Co_3O_4-CeO_2/graphene composite as a novel sensor for amaranth detection. J Electrochem Soc 168:027513

40. Chauhan A, Naseem S, Bahadur J, Singh BR, Shoeb M, Husain S, Khan W (2021) Structural and electrochemical properties of GO/Mn_3O_4 nanocomposite. J Mater Sci-Mater El 32:3894–3902

41. Bandara WRLN, Silva RM, Silva KMN, Dahanayake D, Gunasekara S, Thanabalasingam K (2017) Is nano ZrO_2 a better photocatalyst than nano TiO_2 for degradation of plastics? RSC Adv 7:46155

42. Wei PJ, Li ZH, Zhao XL, Song RM, Zhu ZG (2020) Fe_3O_4/SiO_2/CS surface ion-imprinted polymer modified glassy carbon electrode for highly sensitivity and selectivity detection of toxic metal Ions. J Taiwan Inst Chem E 113:107–113

43. Lu Y, Xie X, Fang W (2020) Insight into the property modification of Zr-incorporated alumina binary mixed oxides by XRD, TEM, XPS, TPD and IR. ChemistrySelect 5:7928–7933

44. Lv X, Yang GJ, Feng C, Lin T (2022) Highly sensitive humidity sensor based on the solid solution $Zr_{0.2}Ti_{0.8}O_2$ nanofibers. J Alloy Compd 891:161958

45. Sun Z, Zhang X, Na N, Liu ZM, Han BX, An GM (2006) Synthesis of ZrO_2-carbon nanotube composites and their application as chemiluminescent sensor material for ethanol. J Phys Chem B 110:13410–13414

46. Asha JB, Suresh P (2020) Covalently modified graphene oxide as highly fluorescent and sustainable carbonaceous chemosensor for selective detection of zirconium ion in complete aqueous medium. ACS Sustain Chem Eng 8:14301–14311

47. Poo-arporn Y, Pakapongpan S, Chanlek N, Poo-arporn RP (2019) The development of disposable electrochemical sensor based on Fe_3O_4-doped reduced graphene oxide modified magnetic screen-printed electrode for ractopamine determination in pork sample. Sensor Actuat B-Chem 284:164–171

48. Xu J, Yang H, Fu W, Sui Y, Zhu H, Li M, Zou G (2006) Preparation and characterization of carbon fibers coated by Fe_3O_4 nanoparticles. Mat Sci Eng B-Adv 132:307–310

49. Meng HL, Lin SY, Feng JJ, Zhang L, Wang AJ (2022) Coordination regulated pyrolysis synthesis of ultrafine $FeNi/(FeNi)_9S_8$ nanoclusters/nitrogen, sulfur-codoped graphitic carbon nanosheets as efficient bifunctional oxygen electrocatalysts. J Colloid Interface Sci 610:573–582

50. Chen YP, Lin SY, Sun RM, Wang AJ, Zhang L, Ma XH, Feng JJ (2022) FeCo/FeCoP encapsulated in N, Mn-codoped three-dimensional fluffy porous carbon nanostructures as highly efficient bifunctional electrocatalyst with multi-components synergistic catalysis for ultra-stable rechargeable Zn-air batteries. J Colloid Interface Sci 605:451–462

51. Zhang L, Ma YT, Duan JJ, Yao YQ, Feng JJ, Wang AJ (2022) In-situ construction of 3D hetero-structured sulfur-doped nanoflower-like FeNi LDH decorated with NiCo Prussian blue analogue cubes as efficient electrocatalysts for boosting oxygen evolution reaction. J Colloid Interface Sci 611:205–214

52. Han Z, Feng JJ, Yao YQ, Wang ZG, Zhang L, Wang AJ (2021) Mn, N, P-tridoped bamboo-like carbon nanotubes decorated with ultrafine $Co_2P/FeCo$ nanoparticles as bifunctional oxygen electrocatalyst for long-term rechargeable Zn-air battery. J Colloid Interface Sci 590:330–340

53. Liu Z, Liu D, Zhao LY, Tian JQ, Yang J, Feng LG (2021) Efficient overall water splitting catalyzed by robust $FeNi_3N$ nanoparticles with hollow interiors. J Mater Chem A 9(12):7750–7758

54. Liu Z, Tang B, Gu XC, Liu H, Feng LG (2020) Selective structure transformation for $NiFe/NiFe_2O_4$ embedded porous nitrogen-doped carbon nanosphere with improved oxygen evolution reaction activity. Chem Eng J 395:125170

55. Zhang S, Xu F, Liu ZQ, Chen YS, Luo YL (2019) Novel electrochemical sensors from poly [N-(ferrocenyl formacyl) pyrrole]@multi-walled carbon nanotubes nanocomposites for simultaneous determination of ascorbic acid, dopamine and uric acid. Nanotechnology 31:085503

56. Deng X, Lee J, Matranga C (2010) Preparation and characterization of $Fe_3O_4(1\ 1\ 1)$ nanoparticles and thin films on Au(1 1 1). Surf Sci 604:627–632

57. Zhu SC, Yang Y, Chen KX, Su ZL, Wang JJ, Li SJ, Song NN, Luo SP, Xie AJ (2022) Novel cubic gravel-like $EDAPbCl_4@ZIF$-67 as electrochemical sensor for the detection of protocatechuic acid. J Alloy Compd 903:163946

58. Yan Y, Bo XJ, Guo LP (2020) MOF-818 metal-organic framework-reduced graphene oxide/multiwalled carbon nanotubes composite for electrochemical sensitive detection of phenolic acids. Talanta 218:121123

59. Yang Y, Li MX, Zhu ZW (2019) A novel electrochemical sensor based on carbon nanotubes array for selective detection of dopamine or uric acid. Talanta 201:295–300

60. Puangjan A, Chaiyasith S (2016) An efficient ZrO_2/Co_3O_4/reduced graphene oxide nanocomposite electrochemical sensor for simultaneous determination of gallic acid, caffeic acid and protocatechuic acid natural antioxidants. Electrochim Acta 211:273–288

61. Abdel-Hamid R, Bakr A, Newair EF, Garcia F (2019) Simultaneous voltammetric determination of gallic and protocatechuic acids in mango juice using a reduced graphene oxide-based electrochemical sensor. Beverages 5:17

62. Gao F, Cai XL, Wang X, Gao C, Liu SL, Gao F, Wang QX (2013) Highly sensitive and selective detection of dopamine in the presence of ascorbic acid at graphene oxide modified electrode. Sens Actuator B Chem 186:380–387

63. Huang HP, Yue YF, Chen ZZ, Chen YN, Wu SZ, Liao JS, Liu S, Wen HR (2019) Electrochemical sensor based on a nanocomposite prepared from $TmPO_4$ and graphene oxide for simultaneous voltammetric detection of ascorbic acid, dopamine and uric acid. Microchim Acta 189:186

64. Bao Y, Song JX, Mao Y, Han DX, Yang F, Niu L, Ivaska A (2011) Graphene oxide-templated polyaniline microsheets toward simultaneous electrochemical determination of AA/DA/UA. Electroanaly 23:878

65. Kumar M, Swamy K, Asif M, Viswanath CC (2017) Preparation of alanine and tyrosine functionalized graphene oxide nanoflakes and their modified carbon paste electrodes for the determination of dopamine. Appl Surf Sci 399:411–419

66. Han DX, Han TT, Shan CS, Ivaska A, Niu L (2010) Simultaneous determination of ascorbic acid, dopamine and uric acid with chitosan-graphene modified electrode. Electroanal 22:2001–2008

67. Skeika T, Zuconelli CR, Fujiwara ST, Pessoa CA (2011) Preparation and electrochemical characterization of a carbon ceramic electrode modified with ferrocenecarboxylic acid. Sensors 11:1361–1374

68. Zhang X, Gu SQ, Ding YP (2014) Simultaneous detection of roxithromycin and dopamine using a sensor platform based on poly(sulfosalicylic acid) and its application in human serum studies. Anal Methods-Uk 6:3316–3321

69. Harish S, Mathiyarasu J, Phani KLN, Yegnaraman V (2008) PEDOT/Palladium composite material: synthesis, characterization and application to simultaneous determination of dopamine and uric acid. J Appl Electrochem 38:1583–1588